Supplement of

Simultaneous measurements of gas- and aerosol-phase water-soluble organic nitrogen in the winter urban atmosphere of Chengdu, China

Kaitao Chen et al.

Correspondence to: Prof. Gehui Wang, Email：ghwang@geo.ecnu.edu.cn

Text S1. Detailed description of the online measurement by the IGAC and method accuracy test.

Ambient air is sampled through a $PM_{2.5}$ sharp-cut cyclone at a flow rate of 16.7 L min^{-1}, and then passes sequentially through a wet annular denuder (WAD) where gaseous compounds are absorbed into pure water, and a scrub and impactor aerosol collector (SIC) where $PM_{2.5}$ are collected and transformed into liquid samples. The collected gas and aerosol samples, after removal of insoluble species and bubbles, are injected into an ion chromatography system (ICS–5000+) for determination of water-soluble inorganic ions and small molecular amines (e.g., methylamine (MA), dimethylamine (DMA)), while the remaining portions are simultaneously analyzed by a TOC/TN analyzer (TOC–L CPH).

WSOC is determined by difference: total carbon (TC) is measured via high-temperature (680°C) Pt-catalyzed combustion converting all carbon to CO_2 detected by non-dispersive infrared (NDIR), yielding water-soluble total carbon (WSTC); inorganic carbon (IC) is measured after acidification with 25% H_3PO_4 converting inorganic carbonates to CO_2 detected by NDIR, yielding water-soluble inorganic carbon (WSIC); WSOC is calculated as WSTC minus WSIC. Similarly, WSON is obtained as the difference between water-soluble total nitrogen (WSTN) measured by combustion and water-soluble inorganic nitrogen (WSIN, mainly ammonium, nitrate, and nitrite) determined by ion chromatography. Calibration curves for TC and IC are established using standard solutions of $NaHCO_3$, Na_2CO_3, and potassium hydrogen phthalate. The calibration curve for total nitrogen was created using a KNO_3 standard solution.

Text S2. Calculation of the contributions of the major components of $PM_{2.5}$ to ALWC.

Inorganic ALWC was simulated using the ISORROPIA-II thermodynamic model, constrained by ambient meteorological parameters and measured concentrations of

inorganic ions. The contribution of $(NH_4)_2SO_4$ to total ALWC was isolated by calculating the difference between the full model prediction and a simulation excluding $(NH_4)_2SO_4$ input (i.e., setting $((NH_4)_2SO_4 = 0)$. Similarly, the contribution of NH_4NO_3 was derived from the difference in ALWC between simulations performed with and without NH_4NO_3 (i.e., setting $NH_4NO_3 = 0$). The equation for $ALWC_{org}$ is as follows (Lv et al., 2022a; Lv et al., 2022b):

$$ALWC_{org} = \frac{[OM]\rho_w}{\rho_{org}} \frac{\kappa_{org}}{\frac{1}{RH} - 1} \quad \text{(S1)}$$

Where [OM] is the concentration of fine particulate organic matter ($OM = OC \times 1.6$); ρ_w and ρ_{org} are the density of water (ρ_w= 1.0 g cm^{-3}) and OM (ρ_{org}= 1.4 g cm^{-3}), respectively; and κ_{org} is the hygroscopicity parameter for organic aerosol composition (κ_{org} = 0.06).

Text S3. The dependencies of amines on pH, ALWC, and T (S-curve equation derivations)

3.1 CH_3NH_2–$CH_3NH_3^+$ partitioning

Here, we show the detailed derivation of equation (4) in that paper. The equilibrium between gaseous CH_3NH_2 and particle-phase $CH_3NH_3^+$ involves two processes: First, CH_3NH_2 dissolves into the aqueous phase (assuming the particles are liquids). Second, dissolved CH_3NH_2 undergoes hydrogenation (H^+) to form $CH_3NH_3^+$. The two processes are reversible and often reach thermodynamic equilibriums at ambient conditions (RH, T) for fine particles.

1st	$CH_3NH_2(g) \leftrightarrow CH_3NH_2(aq)$	$H_{CH_3NH_2}$
2nd	$CH_3NH_2(aq) + H^+(aq) \leftrightarrow CH_3NH_3^+(aq)$	$1/K_a$

for which reaction equilibriums are expressed as follows,

$$H_{CH_3NH_2} = \gamma_{CH_3NH_2}[CH_3NH_2]/p_{CH_3NH_2} \quad \text{(S2)}$$

$$1/K_a = \frac{\gamma_{CH_3NH_3^+}[CH_3NH_3^+]}{\gamma_{CH_3NH_2}[CH_3NH_2]\gamma_{H^+}[H^+]} \quad \text{(S3)}$$

where, $H_{CH_3NH_2}$ is CH_3NH_2 Henry's law constant ($H_{CH_3NH_2} = 90.179\ mol\ atm^{-1}\ kg^{-1}$, 298.15 K) (Sander, 2023), K_a is $CH_3NH_3^+$ acid dissociation constant ($K_a = 2.1878 \times 10^{-11}\ mole\ L^{-1}$, 298.15 K) (Ge et al., 2011), γ_i represents activity coefficient, $p_{CH_3NH_2}$ is partial pressure of CH_3NH_2 in atmosphere, and [x] represents aqueous concentrations (mole L^{-1}). Please note that methylamine is an organic amine classified as a weak base. When methylamine comes into contact with water, a reaction similar to that between ammonia and water occurs (Fountoukis and Nenes, 2007). Methylamine can accept a proton (H^+) from water. In this reaction, methylamine acts as a base, causing water to dissociate and produce hydroxide ions (OH^-). The reaction is represented by the equation:

$$2^{nd} \qquad CH_3NH_2(aq) + H_2O(aq) \leftrightarrow CH_3NH_3^+(aq) + OH^-(aq) \qquad K_w/K_a$$

where K_w is water dissociation constant. Equations (S2) and (S3) give the total dissolved CH_3NH_2 or total particle-phase methylammonium ion ($[CH_3NH_3^T]$) as

$$[CH_3NH_3^T] = [CH_3NH_2] + [CH_3NH_3^+] = H_{CH_3NH_2}p_{CH_3NH_2}\left(\frac{1}{\gamma_{CH_3NH_2}} + \frac{\gamma_{H^+}[H^+]}{\gamma_{CH_3NH_3^+}K_a}\right) \quad \text{(S4)}$$

Combining with ideal gas law, that is

$$c[CH_3NH_2] = \frac{p_{CH_3NH_2}}{RT} \quad \text{(S5)}$$

Where $c[x]$ is concentration per volume of air , R is the gas constant, and T is the temperature. Therefore, the particle-phase fraction of the methylammonium ion is:

$$\varepsilon(CH_3NH_3^+) = \frac{c(CH_3NH_3^T)}{c(CH_3NH_2) + c(CH_3NH_3^T)} = \frac{[CH_3NH_3^T]\,W_i}{c(CH_3NH_2) + [CH_3NH_3^T]\,W_i} \quad \text{(S6)}$$

where W_i is the liquid water content of the particles (μg m^{-3}; mass per volume of air). Taking equations (S4) and (S5) into (S6), we get $\varepsilon(CH_3NH_3^T)$ as

$$\varepsilon\left(CH_3NH_3{}^+\right) = \frac{\left(\frac{\gamma_{H^+}[H^+]}{\gamma_{CH_3NH_3{}^+}} + \frac{K_a}{\gamma_{CH_3NH_2}}\right)\frac{H_{CH_3NH_2}}{K_a}W_iRT}{1 + \left(\frac{\gamma_{H^+}[H^+]}{\gamma_{CH_3NH_3{}^+}} + \frac{K_a}{\gamma_{CH_3NH_2}}\right)\frac{H_{CH_3NH_2}}{K_a}W_iRT} \quad \text{(S7)}$$

To be consistent with the SI units and substitute $[H^+] = 10^{-pH}$, equation (S7) is presented as:

$$\varepsilon\left(CH_3NH_3{}^+\right) = \frac{\left(\frac{\gamma_{H^+}}{\gamma_{CH_3NH_3{}^+}}10^{-pH} + \frac{K_a}{\gamma_{CH_3NH_2}}\right)\frac{H_{CH_3NH_2}}{K_a}W_iRT \times 0.987 \times 10^{-14}}{1 + \left(\frac{\gamma_{H^+}}{\gamma_{CH_3NH_3{}^+}}10^{-pH} + \frac{K_a}{\gamma_{CH_3NH_2}}\right)\frac{H_{CH_3NH_2}}{K_a}W_iRT \times 0.987 \times 10^{-14}} \quad \text{(S8)}$$

Please note that 0.987×10^{-14} is derived from the use of $R = 8.314\, m^3\, Pa\, K^{-1}\, mole^{-1}$, so 1 atm and 1 L must be converted to 1 Pa and 1 μg, respectively.

3.2 $(CH_3)_2NH$ –$(CH_3)_2NH_2^+$ partitioning

Following the same derivation procedure as CH_3NH_2 –$CH_3NH_3^+$ partitioning, we have $\varepsilon((CH_3)_2NH_2^+)$ as

$$\varepsilon\left((CH_3)_2NH_2{}^+\right) = \frac{\left(\frac{\gamma_{H^+}}{\gamma_{(CH_3)_2NH_2{}^+}}10^{-pH} + \frac{K_a}{\gamma_{(CH_3)_2NH}}\right)\frac{H_{(CH_3)_2NH}}{K_a}W_iRT \times 0.987 \times 10^{-14}}{1 + \left(\frac{\gamma_{H^+}}{\gamma_{(CH_3)_2NH_2{}^+}}10^{-pH} + \frac{K_a}{\gamma_{(CH_3)_2NH}}\right)\frac{H_{(CH_3)_2NH}}{K_a}W_iRT \times 0.987 \times 10^{-14}} \quad \text{(S9)}$$

where, $H_{(CH_3)_2NH}$ is $(CH_3)_2NH$ Henry's law constant ($H_{(CH_3)_2NH}$=56.742 mol atm^{-1} kg^{-1}, 298.15 K) (Sander, 2023), K_a is $(CH_3)_2NH_2^+$ acid dissociation constant ($K_a = 1.8621 \times 10^{-11} mole\, L^{-1}$, 298.15 K) (Ge et al., 2011), γ_i represents activity coefficient.

Table S1. Interannual statistics of $PM_{2.5}$ and its chemical components in the SCB during winter (μg m^{-3}).

Year	$PM_{2.5}$	SO_4^{2-}	NO_3^-	NH_4^+	Cl^-	OM[a]	References
2012	108	22	19	16	—	—	(Chen et al., 2019)
2015	115.41 ± 65.28	25.0	22.7	15.1	—	45.2	(Kong et al., 2020)
2016	195.8 ± 91.0	17.5	25.5	15.8	4.9	60	(Zhang et al., 2024a)
2017	153.9 ± 63.1	11.3	23	12.5	3.9	48	(Zhang et al., 2024a)
2018	119.8 ± 32.0	8.8	17.5	10.8	1.4	35	(Zhang et al., 2024a)
2020	96.1 ± 39.3	7.5	18.5	8.2	1.7	29	(Zhang et al., 2024a)
2021	98.5 ± 38.7	10 ± 4.2	29 ± 14	15.1 ± 6.4	5.2 ± 4.1	39.2 ± 3.9[b]	(Bao et al., 2023)
2023	95.6 ± 28.7	8.8	21.0	7.5	1.7	33.7	(Zhang et al., 2024b)
2024	76 ± 38	4.9 ± 2.0	16.7 ± 8.3	7.2 ± 3.0	1.3 ± 1.0	21.1 ± 9.6	this study

[a] $OM = OC \times 1.6$. [b]Obtained via ToF-ACSM.

Table S2. Daytime and nighttime concentrations and gas-particle partitioning of WSON during clean, transition, and pollution haze periods (μg m^{-3}).

		Daytime				Nighttime				p[b]
		Mean	Median	SD[a]	Range	Mean	Median	SD	Range	
Clean Period	$WSON_g$[c]	0.63	0.46	0.56	0.13–1.46	0.68	0.57	0.53	0.06–1.71	$p > 0.05$
	$WSON_p$[c]	0.76	0.78	0.27	0.36–1.09	1.13	0.82	1.11	0.11–4.35	$p > 0.05$
	F_{WSON}[d]	0.62	0.67	0.25	0.29–0.88	0.61	0.61	0.07	0.51–0.72	$p > 0.05$
Transition Period	$WSON_g$	1.23	1.18	0.79	0.33–3.91	0.76	0.63	0.52	0.14–2.15	$p < 0.01$
	$WSON_p$	1.68	1.47	0.94	0.16–4.90	1.42	1.25	0.66	0.12–2.90	$p > 0.05$
	F_{WSON}	0.60	0.64	0.15	0.28–0.87	0.71	0.71	0.12	0.53–0.90	$p < 0.01$
Pollution Period	$WSON_g$	1.85	1.52	1.25	0.21–5.82	1.05	0.86	0.74	0.09–3.17	$p < 0.001$
	$WSON_p$	3.45	3.74	1.42	0.33–6.19	2.71	2.48	1.31	0.78–6.34	$p < 0.01$
	F_{WSON}	0.69	0.69	0.13	0.42–0.90	0.76	0.75	0.12	0.42–0.98	$p < 0.01$

[a] Standard Deviation. [b] Statistical Significance (p-values <0.05 considered statistically significant). [c] Concentration of water-soluble organic nitrogen (WSON) in the gas-phase (g) and particulate-phase (p). [d] Gas-particle partitioning of WSON.

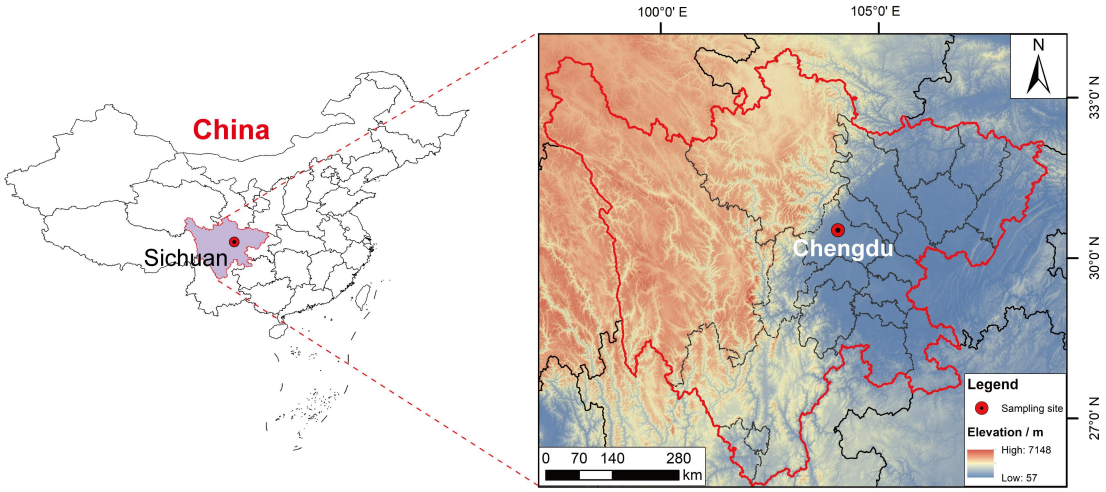

96

97 **Figure S1.** Geographic location of the sampling site in Sichuan Basin (SCB), China.

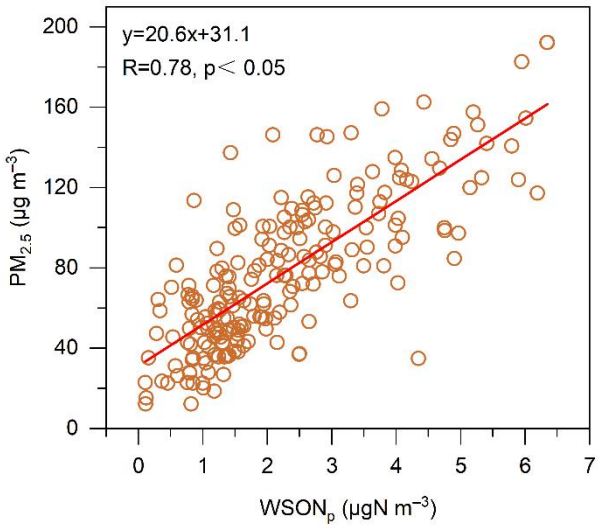

98

99 **Figure S2.** Correlation Scatter Plot Between $WSON_p$ and $PM_{2.5}$.

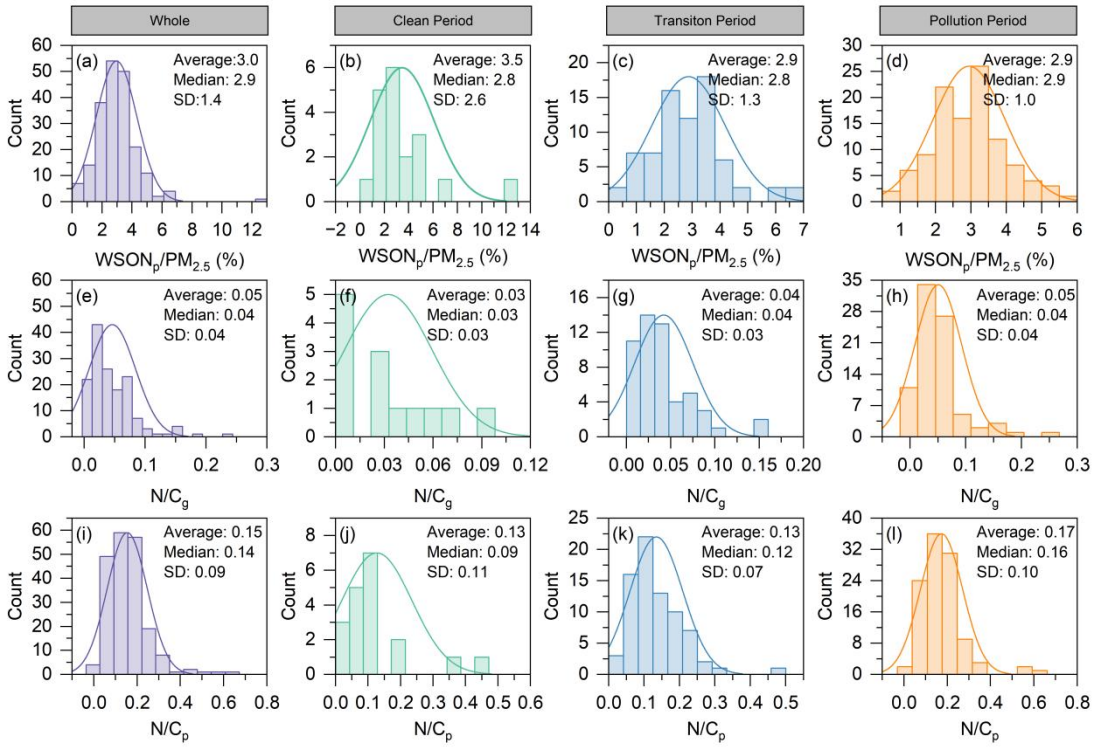

Figure S3. Frequency distribution characteristics of WSON contribution and nitrogen to carbon (WSON/WSOC) ratios in $PM_{2.5}$ during different periods. (a–d) Mass percentage of water-soluble organic nitrogen in $PM_{2.5}$ ($WSON_p/PM_{2.5}$, %); (e–h) Molar ratio of nitrogen to carbon in the gas phase ($WSON/WSOC_g$); (i–l) Molar ratio of nitrogen to carbon in the particle phase ($WSON/WSOC_p$). The solid lines represent Gaussian distribution fits to the data. The average, median and standard deviation (SD) for each dataset are indicated in the panels.

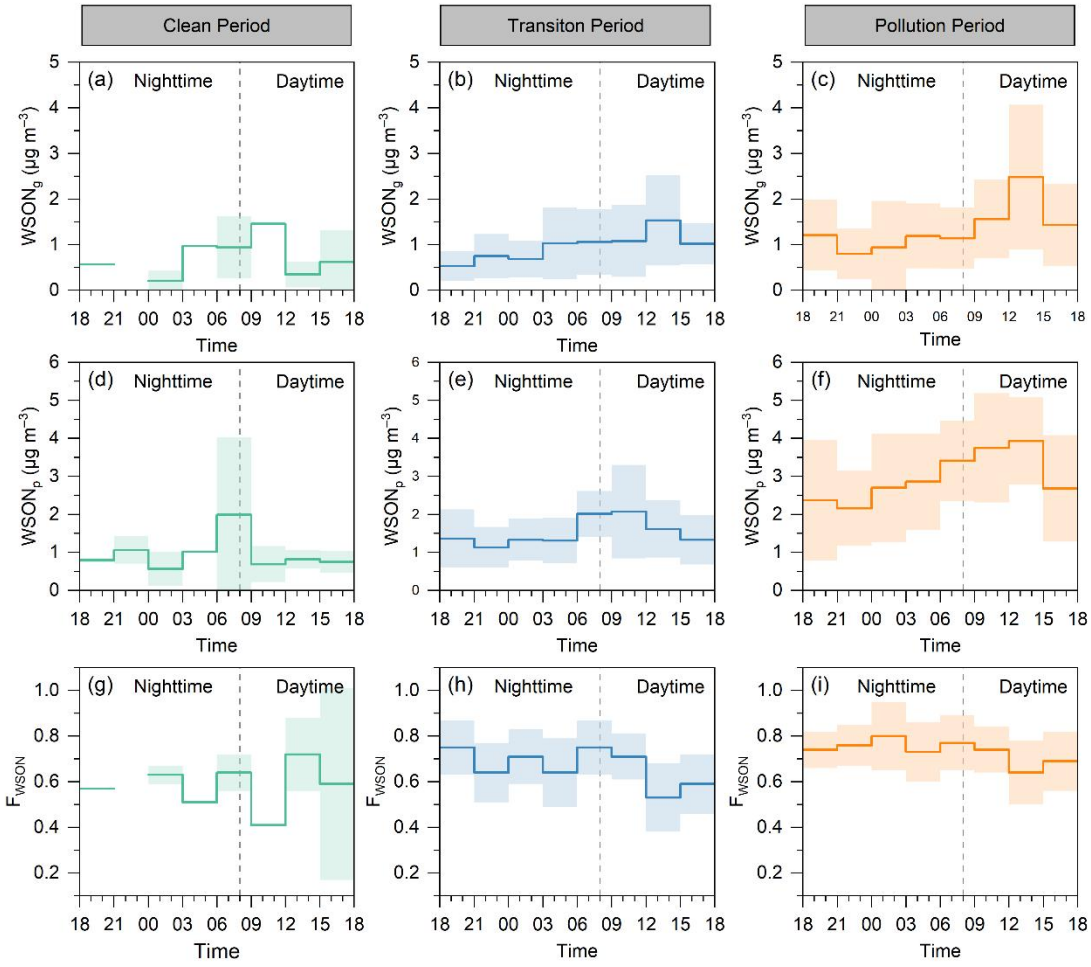

Figure S4. Diurnal variations of WSON and gas-particle partitioning during clean, transition, and pollution periods. Here, a, b, c and d, e, f represent the diurnal variation concentrations of gas and particle phase, respectively, and g, h, i represent the partition coefficient of WSON (F_{WSON}). The time shown is Beijing Time.

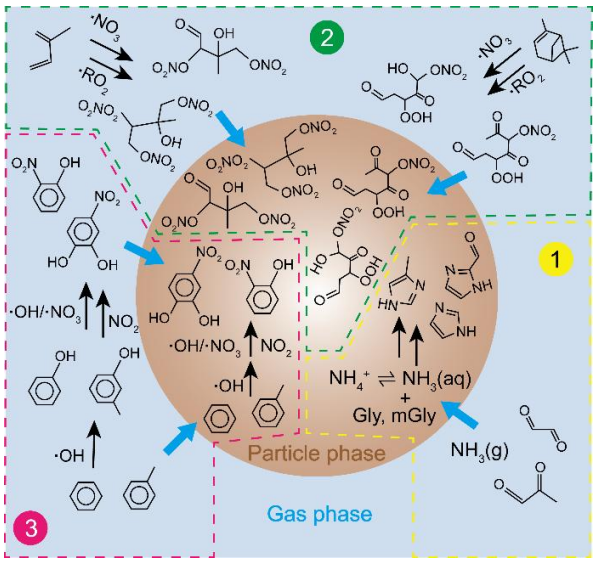

Figure S5. Secondary generation path of WSON (Zhang et al., 2026; Xiao et al., 2025; Vione et al., 2004; Yuan et al., 2016; Wang et al., 2019; Chen et al., 2025; Liu et al., 2023).

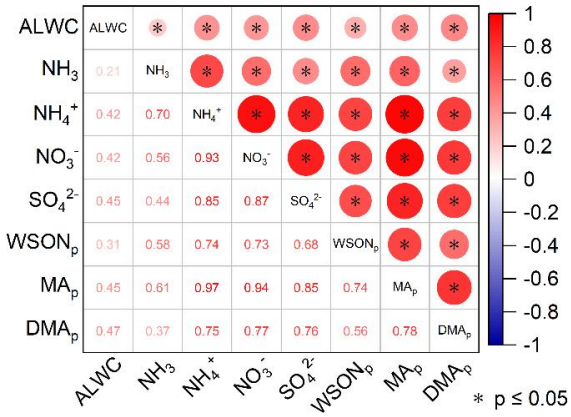

Figure S6. Factors affecting the concentration of $WSON_p$, methylamine$_p$ (MA_p) and dimethylamine$_p$ (DMA_p) in the SCB region of China.

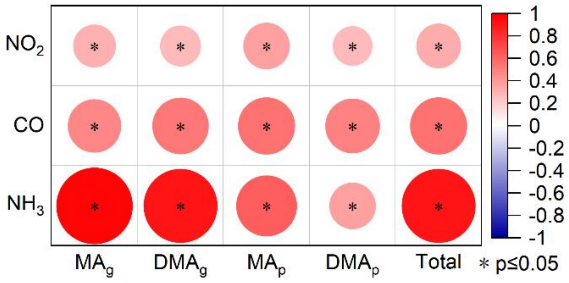

Figure S7. Pearson correlation matrix of gaseous and particulate methylamine (MA) and dimethylamine (DMA) with NH_3, CO, and NO_2 during the wintertime observation in the SCB.

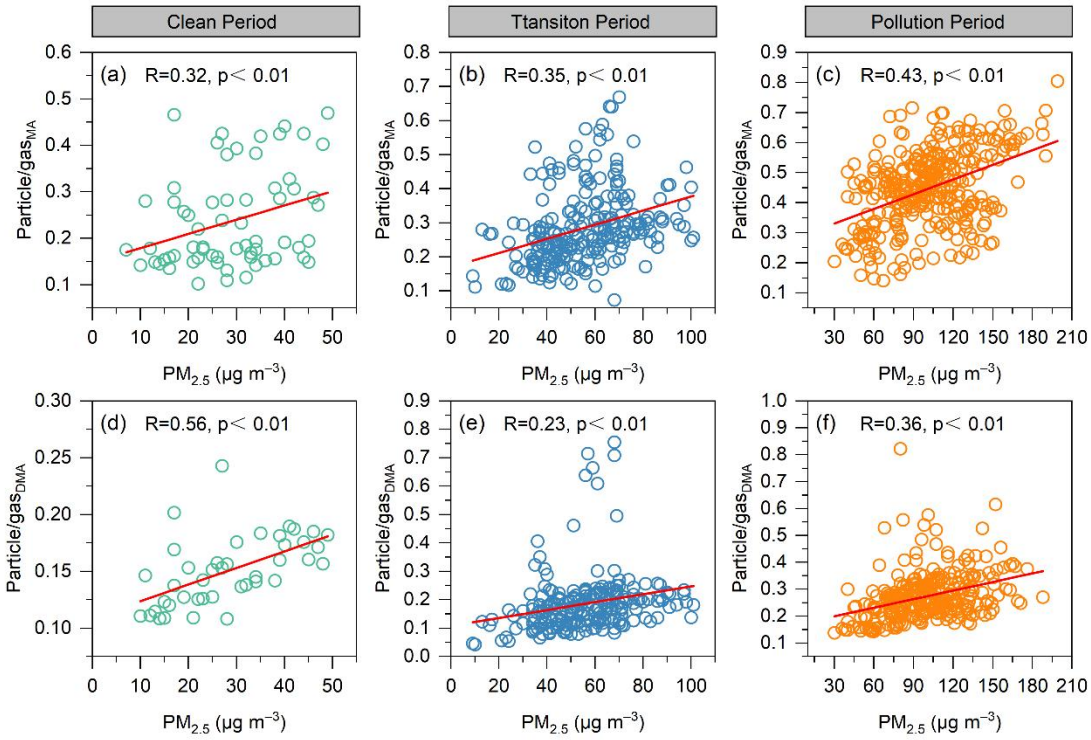

125

126 **Figure S8.** Ratio in particle and gas phase signal of the methylamine (MA) and
127 dimethylamine (DMA)–versus total $PM_{2.5}$ concentration (μg m^{-3}) for all observations
128 during the campaign. According to equation (10), the slope of a linear fit will provide
129 K_i for the selected constituent.

130

References

Bao, Z., Zhang, X., Li, Q., Zhou, J., Shi, G., Zhou, L., Yang, F., Xie, S., Zhang, D., Zhai, C., Li, Z., Peng, C., and Chen, Y.: Measurement report: Intensive biomass burning emissions and rapid nitrate formation drive severe haze formation in the Sichuan Basin, China – insights from aerosol mass spectrometry, Atmos. Chem. Phys., 23, 1147-1167, https://doi.org/10.5194/acp-23-1147-2023, 2023.

Chen, Y., Xie, S.-d., Luo, B., and Zhai, C.: Characteristics and Sources of Water-Soluble Ions in $PM_{2.5}$ in the Sichuan Basin, China, Atmosphere, 10, https://doi.org/10.3390/atmos10020078, 2019.

Chen, Y., Xia, M., Zheng, P., Li, Y., Zou, Z., Tong, S., Li, K., Feng, X., Hui, L., Yuan, Q., Li, J., Yu, J. Z., Lee, S., Wang, T., and Wang, Z.: Complex gas-particle partitioning of nitro-phenolic compounds: field-based insights and determination of apparent activity coefficient, npj Clim. Atmos. Sci., 8, https://doi.org/10.1038/s41612-025-01156-z, 2025.

Fountoukis, C., and Nenes, A.: ISORROPIA II: a computationally efficient thermodynamic equilibrium model for K^+ –Ca^{2+} –Mg^{2+} –NH_4^+ –Na^+ –SO_4^{2-} –NO_3^- –Cl^- –H_2O aerosols, Atmos. Chem. Phys., 7, 4639–4659, https://doi.org/10.5194/acp-7-4639-2007, 2007.

Ge, X., Wexler, A. S., and Clegg, S. L.: Atmospheric amines – Part II. Thermodynamic properties and gas/particle partitioning, Atmos. Environ., 45, 561-577, https://doi.org/10.1016/j.atmosenv.2010.10.013, 2011.

Kong, L., Tan, Q., Feng, M., Qu, Y., An, J., Liu, X., Cheng, N., Deng, Y., Zhai, R., and Wang, Z.: Investigating the characteristics and source analyses of $PM_{2.5}$ seasonal variations in Chengdu, Southwest China, Chemosphere, 243, https://doi.org/10.1016/j.chemosphere.2019.125267, 2020.

Liu, X., Wang, H., Wang, F., Lv, S., Wu, C., Zhao, Y., Zhang, S., Liu, S., Xu, X., Lei, Y., and Wang, G.: Secondary Formation of Atmospheric Brown Carbon in China Haze: Implication for an Enhancing Role of Ammonia, Environ. Sci. Technol., 57, 11163-11172, https://doi.org/10.1021/acs.est.3c03948, 2023.

Lv, S., Wang, F., Wu, C., Chen, Y., Liu, S., Zhang, S., Li, D., Du, W., Zhang, F., Wang, H., Huang, C., Fu, Q., Duan, Y., and Wang, G.: Gas-to-Aerosol Phase Partitioning of Atmospheric Water-Soluble Organic Compounds at a Rural Site in China: An Enhancing Effect of NH_3 on SOA Formation, Environ. Sci. Technol., 56, 3915-3924, https://doi.org/10.1021/acs.est.1c06855, 2022a.

Lv, S., Wu, C., Wang, F., Liu, X., Zhang, S., Chen, Y., Zhang, F., Yang, Y., Wang, H., Huang, C., Fu, Q., Duan, Y., and Wang, G.: Nitrate-Enhanced Gas-to-Particle-Phase Partitioning of Water-Soluble Organic Compounds in Chinese Urban Atmosphere: Implications for Secondary Organic Aerosol Formation, Environ. Sci. Technol. Lett., 10, 14-20, https://doi.org/10.1021/acs.estlett.2c00894, 2022b.

Sander, R.: Compilation of Henry's law constants (version 5.0.0) for water as solvent, Atmos. Chem. Phys., 23, 10901-12440, https://doi.org/10.5194/acp-23-10901-2023, 2023.

Vione, D., Maurino, V., Minero, C., Lucchiari, M., and Pelizzetti, E.: Nitration and hydroxylation of benzene in the presence of nitrite/nitrous acid in aqueous solution, Chemosphere, 56, 1049-1059, https://doi.org/10.1016/j.chemosphere.2004.05.027, 2004.

Wang, Y., Hu, M., Wang, Y., Zheng, J., Shang, D., Yang, Y., Liu, Y., Li, X., Tang, R., Zhu, W., Du, Z., Wu, Y., Guo, S., Wu, Z., Lou, S., Hallquist, M., and Yu, J. Z.: The formation of nitro-aromatic compounds under high NO_{<i>x</i>} and anthropogenic VOC conditions in urban Beijing, China, Atmos. Chem. Phys., 19, 7649-7665, https://doi.org/10.5194/acp-19-7649-2019, 2019.

Xiao, B., Wang, G., Li, Z., Li, R., Liang, C., Wang, H., Zhang, S., Wu, C., Li, R., Zhang, F., Zhang, R., Wu, Y., and Zhang, L.: High Contribution of Secondary Formation to Brown Carbon in China Humid Haze: Enhancing Role of Ammonia and Amines, Environ. Sci. Technol., 59, 27530-27540, https://doi.org/10.1021/acs.est.5c13436, 2025.

Yuan, B., Liggio, J., Wentzell, J., Li, S.-M., Stark, H., Roberts, J. M., Gilman, J., Lerner, B., Warneke, C., Li, R., Leithead, A., Osthoff, H. D., Wild, R., Brown, S. S., and de Gouw, J. A.: Secondary formation of nitrated phenols: insights from observations during the Uintah Basin Winter Ozone Study (UBWOS) 2014, Atmos. Chem. Phys., 16, 2139-2153, https://doi.org/10.5194/acp-16-2139-2016, 2016.

Zhang, J., Li, J., Su, Y., Chen, C., Chen, L., Huang, X., Wang, F., Huang, Y., and Wang, G.: Interannual evolution of the chemical composition, sources and processes of $PM_{2.5}$ in Chengdu, China: Insights from observations in four winters, J. Environ. Sci., 138, 32-45, https://doi.org/10.1016/j.jes.2023.02.055, 2024a.

Zhang, J., Su, Y., Chen, C., Guo, W., Tan, Q., Feng, M., Song, D., Jiang, T., Chen, Q., Li, Y., Li, W., Wang, Y., Huang, X., Han, L., Wu, W., and Wang, G.: Chemical composition, sources and formation mechanism of urban $PM_{2.5}$ in Southwest China: a case study at the beginning of 2023, Atmos. Chem. Phys., 24, 2803-2820, https://doi.org/10.5194/acp-24-2803-2024, 2024b.

Zhang, S., Wang, G., Xu, X., Liu, Y., Nie, W., Chen, L., Li, R., Gao, Y., Li, R., Wu, C., Zhang, J., and Prevot, A. S. H.: Unappreciated Role of Photochemical Aging of Biogenic Organic Nitrates in Atmospheric Ozone Formation, Environ. Sci. Technol., https://doi.org/10.1021/acs.est.5c11688, 2026.